5B.2 VARIABILITY IN THE KINEMATIC STRUCTURE OF SUPER TUESDAY STORMS

Todd A. Murphy* & Kevin R. Knupp
University of Alabama in Huntsville, Huntsville, Alabama

1. INTRODUCTION

Since the advent of multiple Doppler wind retrievals, the meteorological research community has learned a great deal about weather phenomena where direct measurements are often hard to come by. In the late 1970s and 1980s, several techniques were described using Doppler derived winds to retrieve thermodynamic quantities, such as perturbation pressure and buoyancy. One such weather phenomenon where these techniques have been quite useful are the supercell thunderstorm. Although processes within supercells still elude us even today, Doppler wind and thermodynamic retrievals have provided insightful information and even confirmed some suspicions where in situ data is lacking. For example, Cai and Wakimoto (2001) used Doppler derived quantities to confirm how the pressure field influences storm movement.

Often times, one does not have at least two Doppler radars to perform wind retrievals. Bluestein and Hazen (1989) and Klimowski and Marwitz (1992) both describe a technique using single Doppler radars to retrieve the 3-d wind field, which they call the synthetic dual-Doppler (SDD) analysis. Limiting factors of this technique include vector of propagation near the radar site and the quasi-steady-state assumption. The Super Tuesday outbreak of Feb 5-6, 2008, however, provided several cases where a SDD analysis might be successfully applied. Two such cases will be presented here with differing levels of success, one near Nashville, TN (KOHX) and the other Memphis (KNQA). The kinematic structure of both supercells will be examined; specifically the location and strength of certain features, such as the updraft. Thermodynamic retrievals were performed to determine the dominant updraft forcing mechanism. These results, along with concluding remarks of using the SDD method on supercell thunderstorms will be presented.

2. EVENT & CASE OVERVIEW

2.1. *Event*

The Super Tuesday outbreak produced 87 tornadoes, caused 57 fatalities, and hundreds of injuries within a 12-hour period during the evening and early morning hours of 5-6 Feb 2008. The number of fatalities alone was the most in a single outbreak since 1985. Favorable conditions for a significant outbreak began appearing in forecast models days before the event. By 3 Feb, southerly flow induced by strengthening low pressure east of the Rockies and high pressure moving off the east coast provided an ample supply of low-level heat and moisture to the Southeastern United States. By Tuesday, 5 Feb, dew points were nearing 70 °F as far north as Tennessee and Kentucky. This unstable air mass, along with sufficient environmental wind shear aided by the development of a strong low-level jet, provided an environment ripe for supercell development.

During the morning of 5 Feb, a squall line developed across much of Texas ahead of a surface cold front. By 1630 UTC, the Storm Prediction Center (SPC) had outlined large portions of the Mississippi and Ohio river valleys for a moderate risk of severe weather and a portion of that a high risk. The first signs of supercell development began not too long after the SPC convective outlook update, with the first tornado reports occurring near 2200 UTC.

2.2. *Cases*

Two supercells affected the Memphis area near the same time. The first storm, which is not included in this analysis, moved near KNQA between 2245 and 2300 UTC. The time frame for the second storm (case 1) was between 2320 and 0030 UTC, but wasn't close enough to the radar site to begin a SDD analysis until 2336 UTC. This storm developed from a cluster of thunderstorms which initiated in northeast Louisiana and southeast Arkansas near 2000 UTC. They generally moved parallel to the Mississippi River (from ~210°) between 25 and 30 ms^{-1}. By 2230 UTC, cyclonic rotation was evident in a strengthening storm as it crossed the Mississippi River nearing Tunica, MS. As the supercell moved into Tennessee, it produced an EF2 tornado with its track beginning just north of Southaven, MS. This tornado was only the first in what would be a series of tornadoes associated with this supercell (it would later produce a long track EF3 and the EF4 tornado which devastated Union University near Jackson, TN) (Fig. 1). The best SDD analyses were between 2350 and 0020 UTC, when the supercell passed KNQA at a distance of 25-38 km, moving from 230° at 26 ms^{-1}.

The Nashville case (case 2) occurred between 0645 and 0725 UTC, as a supercell just out ahead of a broken line of showers and thunderstorms moved parallel to KOHX. The development of this storm began as a cluster of cells formed in north Mississippi around 0200 UTC. By 0415 UTC, it was already exhibiting signs of a developing mesocyclone on radar as it moved into southern Tennessee and the first "appendage" on radar reflectivity appears near 0500 UTC. As the supercell continued to move to the Northeast (from ~230°), it produced several EF0 tornadoes along its track (Fig. 1). It continued as a tornado producer after passing KOHX and moving into Kentucky, where it was eventually absorbed by the line. The best SDD analyses for this

Corresponding author address: Todd A. Murphy, NSSTC, 320 Sparkman Dr., Huntsville, AL 35805; e-mail: todd.murphy@nsstc.uah.edu

case were between 0650 and 0716 UTC. During this time, the mesocyclone passed KOHX at a distance of 16-25 km, moving from 242° at 24 ms^{-1}.

In both cases, the supercells were well established as they passed the radar sites along the baseline for the SDD analysis. They both had already produced tornadoes and continued to produce them after passing, although no tornado was captured by SDD analyses. The direction and speed of propagation were similar (between 230° and 240° at ~25 ms^{-1}), although case 1 passed south of KNQA and case 2 passed north of KOHX. Also, the mesocyclone in case 1 was 9-14 km further away from the radar. Another difference that needs to be mentioned is supercell strength and coverage. The supercell from the first case was stronger

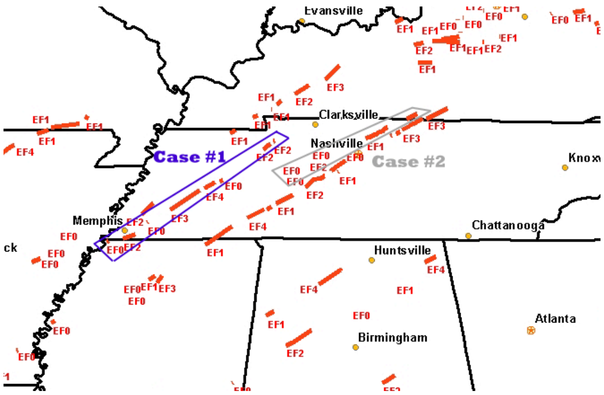

Fig. 1. *Super Tuesday tornado tracks, zoomed in on area of interest for this study. Case 1 is outlined and labeled in blue and case 2 in gray.*

(evident by producing several EF2 and greater tornadoes and stronger rotational velocities on radar) and larger than the second case.

Environmental differences could be the cause of this, since case 1 occurred roughly 7 hours prior to case 2; sunset occurred just before the analysis time for case 1. Due to this, the convective available potential energy (CAPE) decreased between the cases. A modified RUC sounding centered on Nashville, TN for 0700 UTC showed the development of an inversion near the ground, possibly limiting the amount of energy available for this case (Fig. 2). Surface based CAPE (SBCAPE) was less than 500 Jkg^{-1}; however, above the inversion, it was nearing 1000 Jkg^{-1}. For the first case, SBCAPE was greater than 1000 Jkg^{-1}.

3. DATA AND METHODOLOGY

3.1. *Wind Retrieval*

NEXRAD Level II radar data was obtained from the National Climatic Data Center (NCDC). Reflectivity and radial velocity data was edited and dealiased using the NCAR Solo software and interpolated onto a Cartesian grid with 0.5 km spacing using the Reorder software. The data was gridded using the Cressman weighting function with a radius of influence of 1.0 (Cressman 1959). Reflectivity fields common to both volume scans

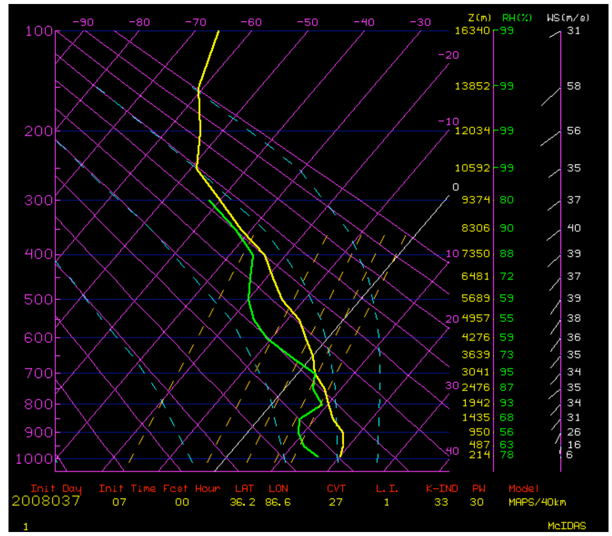

Fig. 2. *Modified RUC sounding, centered on Nashville, TN at 0700 UTC on 6 Feb 2008.*

used in the SDD analysis were matched, and utilizing the GRLevel2 application's storm-motion utility, the translation vector for each storm was found. The actual SDD technique was performed using the common dual-Doppler software, CEDRIC (Mohr et al. 1986).

Klimowski and Marwitz (1992) describe the SDD procedure in detail. Storm-motion must be parallel to the radar site and at a relatively close distance. The feature in question must move quick enough that the angle subtended by it (α) is at least 30°. Additionally, the velocity fields associated with the feature can not significantly change (in this case, the supercell can not weaken or strengthen significantly between volume scans; steady-state assumption). In this analysis, the steadiness of the supercells was first estimated by

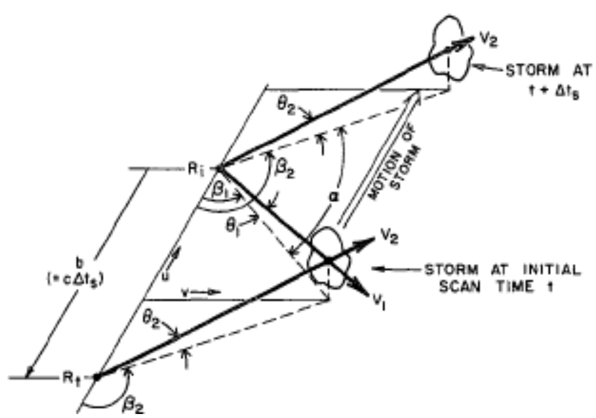

Fig. 3. *Geometry of the synthetic dual-Doppler technique.*

visually comparing the reflectivity structure of several volume scans. If significant changes in structure did not occur, to quantify the steadiness, a correlation analysis of reflectivity fields between volume scans chosen for the SDD analysis was performed.

The dual-Doppler geometry is shown in Fig. 3 (Lhermitte and Miller 1970). The length of the baseline (*b*) is defined as $c\Delta t_s$, where *c* is storm speed and Δt_s is the time between radar volume scans used for the analysis; both cases had a baseline near 30 km. The other variables are defined as follows: R_i - initial radar position, R_t - translated radar position, β - radar azimuth angle, θ - radar elevation angle. Although error can come from many sources during a SDD analysis, the main source is usually changes in radial velocity between the two volume scans. Additionally, error can be introduced through uncertainties in calculating the storm-motion vector, which is used to find the radar baseline.

Once horizontal winds are retrieved, the vertical wind component is found by integrating the mass continuity equation. A variational integration scheme was used, where upper and lower boundary conditions were specified within the column.

For case 2, volume scans at 0655 and 0716 UTC were used for the SDD analysis. Through visual comparison, it appeared that the supercell was not rapidly evolving during this time period. The correlation analysis yielded a correlation coefficient (*r*) between 0.7 and 0.9 for all levels below 6.0 km. Above that, *r* drops to 0.4 and less. For case 1, volume scans at 2359 and 0020 UTC were used, and the visual comparison showed a supercell which was slightly strengthening between volume scans. The correlation analysis yielded a *r* value between 0.4 and 0.7 for elevations below 5 km. Based on these results, the SDD analysis for case 2 should contain *less* error than case 1.

3.2. *Thermodynamic Retrieval*

Once the three-dimensional wind field is known, by basically rearranging the momentum equations, one can solve for pressure. Although not quite as simple as it sounds, the result of performing an analysis similar to this is an *estimate* of the pressure (and buoyancy if one chooses) perturbation field. Gal-Chen (1978) pioneered the retrieval of thermodynamic variables from observed winds while others have used and modified the procedure (Hane et al. 1981; Pasken and Lin 1982; Brandes 1984; Roux 1985; Hane and Ray 1985). The method performed here is in the same fashion as that done by the others listed.

Rearrange the horizontal momentum equations to solve for pressure using the "known" quantities (F and G):

$$\frac{\partial p'}{\partial x} = -\rho_o \frac{Du}{Dt} + fr_x \equiv F \tag{1}$$

$$\frac{\partial p'}{\partial y} = -\rho_o \frac{Dv}{Dt} + fr_y \equiv G \tag{2}$$

A solution for *p'* can be found only if:

$$\frac{\partial F}{\partial y} = \frac{\partial G}{\partial x} \tag{3}$$

Since the friction terms (fr_x, fr_y) and total derivatives are imperfect and not determined exactly, *p'* can only be found using a least-squares solution which leads to:

$$\frac{\partial^2 p'}{\partial x^2} + \frac{\partial^2 p'}{\partial y^2} = \frac{\partial F}{\partial x} + \frac{\partial G}{\partial y} \tag{4}$$

This partial differential equation is a Poisson equation, which is subject to Neumann boundary conditions. The known quantities (F and G) are acquired from the SDD wind retrieval.

Buoyancy is found using the equation:

$$\begin{aligned} B &= \frac{(\theta - <\theta>)}{\theta} + 0.61(q_v - <q_v>) \\ &= \frac{c_p \theta_v}{g} \frac{\partial (p' - <p'>)}{\partial z} + R - <R> \end{aligned} \tag{5}$$

where

$$R = \frac{1}{g}\frac{Dw}{Dt} + q_c + q_r$$

A sounding from each location was used to find θ_v, q_c, and q_r, where q_c and q_r are cloud water and rain water mixing ratios, respectively.

Given that a steady-state assumption is applied for the SDD analysis, time derivatives are set to 0. This introduces some error in the thermodynamic retrieval. The buoyancy equation assumes the cloud is free of ice, so since this analysis deals with supercells, hail is more than likely present. This also introduces error into the buoyancy analysis.

4. RESULTS

4.1. *Case 1*

Examples from the two gridded volume scans used in the SDD analysis is seen in Fig. 4. It's obvious the storm was evolving during the scan period, introducing some error into the analysis. By the time volume scan 2 occurred, the supercell developed a well defined BWER as low as 2.0 km, indicating a strengthening mesocyclone. Even with the evolving nature of the storm, a SDD analysis was still performed. However, due to a low correlation between reflectivity's above 5 km, only elevations at that height and below were considered for this analysis.

Average reflectivity (DZA; reflectivity of both volume scans averaged) overlain with the horizontal wind vectors shows a well defined mesocyclone at 1.5, 3.0, and even 4.0 km (Fig. 5). Strong inflow and convergence along what should be the rear flank gust front is also very prominent at 1.5 km. Data along the radar baseline (near the upper-left corner) is suspect to error. There also appears to be some suspect data within the forward-flank at 3.0 and 4.0 km. Overall however, positions of notable features appear fair for the analysis.

In the lowest 5 km, vertical motion peaks near 50 ms^{-1} at 4.0 km (Fig. 6). Vertical velocities ≥ 10 ms^{-1} tend to de-mark the location of the rear flank gust front (a

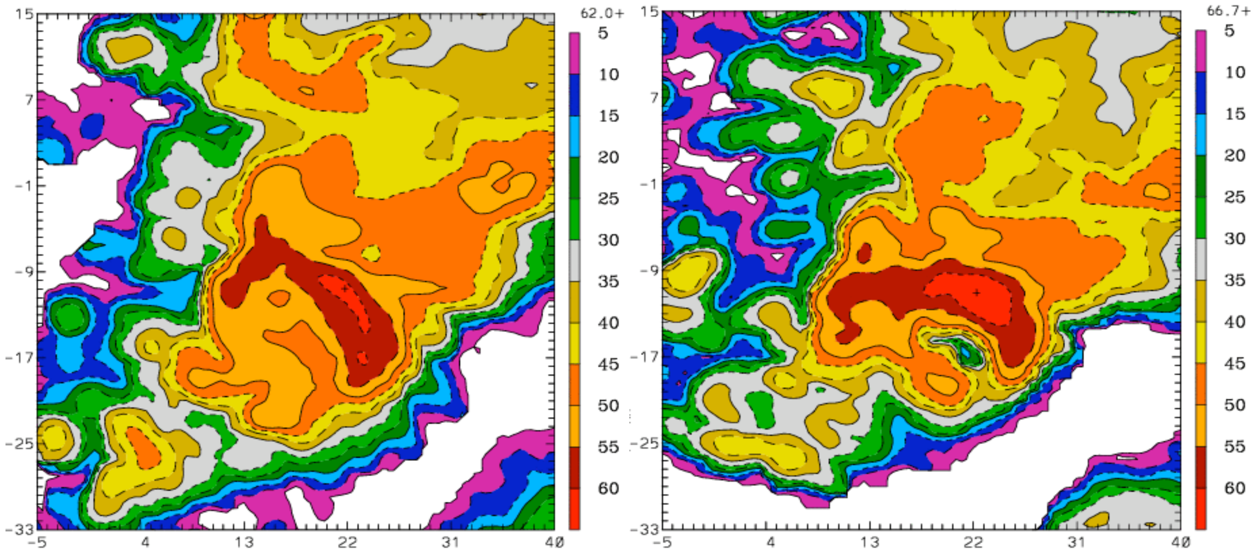

Fig. 4. *KNQA volume scan 1 (2359 UTC; left image) and volume scan 2 (0020 UTC; right image) taken at 3.0 km. Used for steadiness comparison between volume scans.*

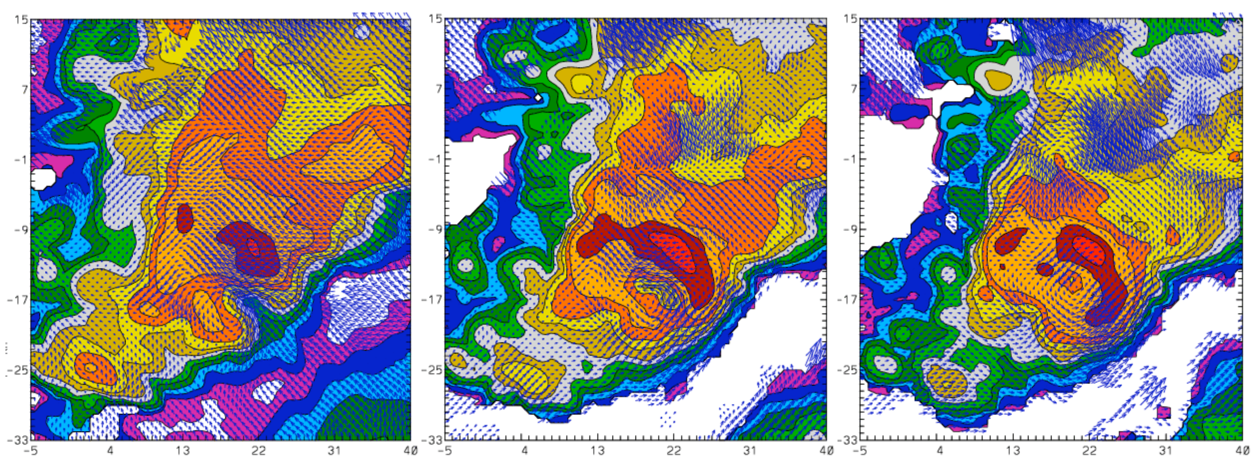

Fig. 5. *SDD analysis at 1.5, 3.0, and 4.0 km for case 1. Reflectivity scale is same as Fig. 4. Horizontal wind vectors are overlain. Reference vector -* 20 M/S

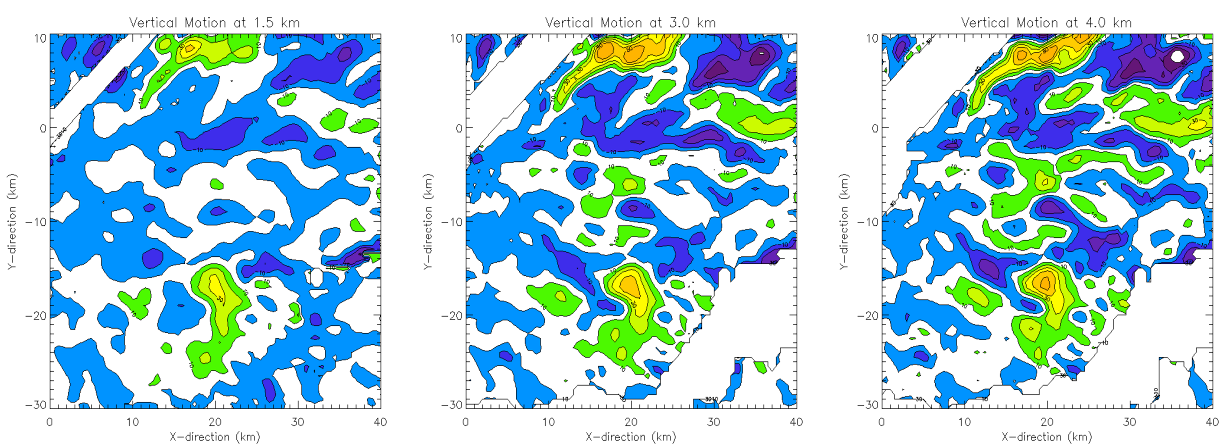

Fig. 6. *Vertical motion at 1.5, 3.0, and 4.0 km for case 1. Warm colors are positive (upward motion) and cool colors are negative (downward motion). Contour interval is 10 ms^{-1} and green is ≥ +10 ms^{-1} . Note that Fig. 5 and 6 are not quite on the same scale.*

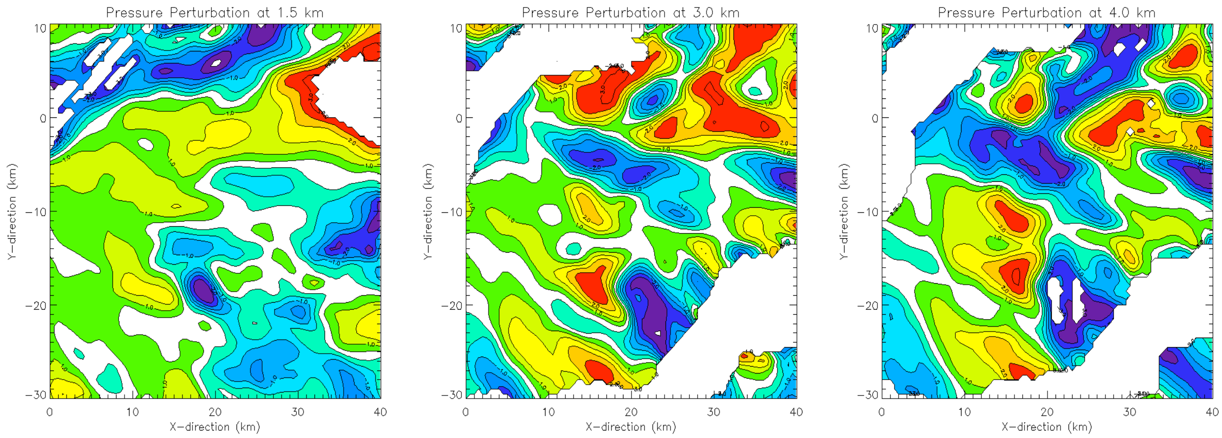

Fig. 7. *Pressure perturbation at 1.5, 3.0, and 4.0 km for case 1. Cool colors represent a negative perturbation while warm colors are positive. The contour interval is 0.5 hPa. The seemingly data void region at 4.0 km within the negative perturbations is actually the -3.0 hPa contour.*

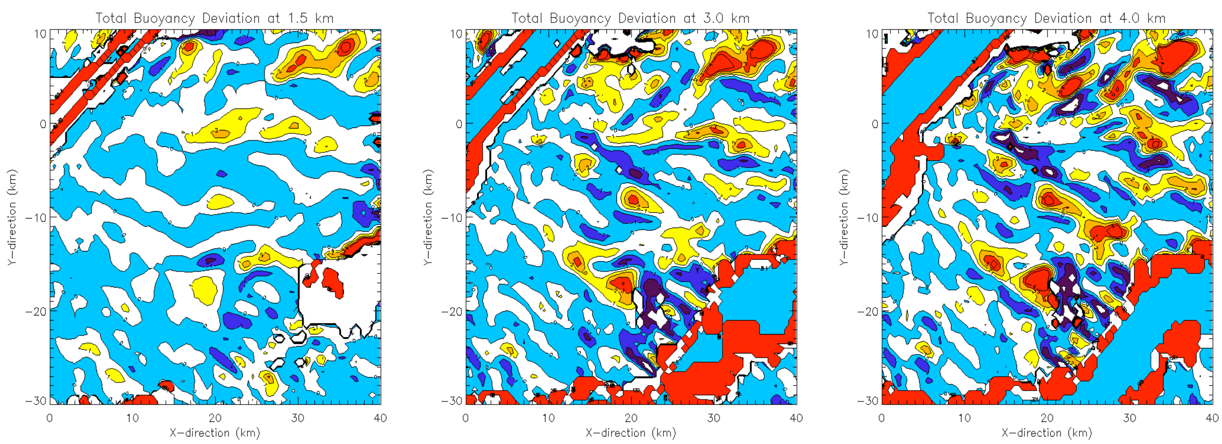

Fig. 8. *Total buoyancy deviations at 1.5, 3.0, and 4.0 km for case 1. Cool colors represent a negative deviation while warm a positive deviation. The contour interval is 1°.*

focal point for new updraft generation). Vertical velocities within the rear-flank downdraft (RFD) also shows up quite well as an area with vertical velocities ≤ -10 ms^{-1}. Again, features near the baseline must be ignored.

The lowest pressure perturbations are on the order of -3.0 hPa at 4.0 km (the level of the updraft maximum). This meso-low pressure at 4.0 km suggests that a vertical pressure gradient was set up, helping maintain the updraft. Positive pressure perturbations within the rear-flank are on the order of 1.5 - 3.0 hPa.

Buoyancy forcing also seems to play a prominent role, as total buoyancy deviations are on the order of +4.0 K (or °C) and greater near the level of maximum vertical motion (Fig. 8). The buoyancy fields are quite noisy, especially near boundaries (such as the radar baseline) and near areas which lack data. This is partially because of the vertical pressure perturbation gradient, which is required in equation 5. Due to some clear air around the supercell (lacking reflectivity/velocity data), the pressure perturbation equation was unable to solve for *p'*, therefore unreliable buoyancy calculations were made in those regions.

4.2. *Case 2*

Gridded volume scans used for this analysis shows very little evolution between scan times. An example of the gridded scans taken at 3.0 km is seen in Fig. 9. Similar to case 1, due to a lower correlation for variables above 6 km, only elevations from that height and lower are considered. Overall, it appears this supercell was evolving much more slowly than case 1 (especially at lower levels), better satisfying the steady-state assumption. The quality of this analysis is expected to be better than case 1.

Results from the SDD analysis (Fig. 10) shows a well defined mesocyclone in the horizontal wind field, but not as strong as case 1. Placement of the mesocyclone within the reflectivity core seems correct. Storm inflow is strong at 1.5 km and matches up well with the “inflow notch” in the reflectivity field. The strong wind near the bottom of the figure are along the radar baseline and should be discarded. There doesn’t seem to be as much (if any) suspect data with this analysis.

Vertical motion peaks at 34.5 ms^{-1} at 3.0 km (Fig. 11). This is about 15 ms^{-1} and a full 1 km lower than

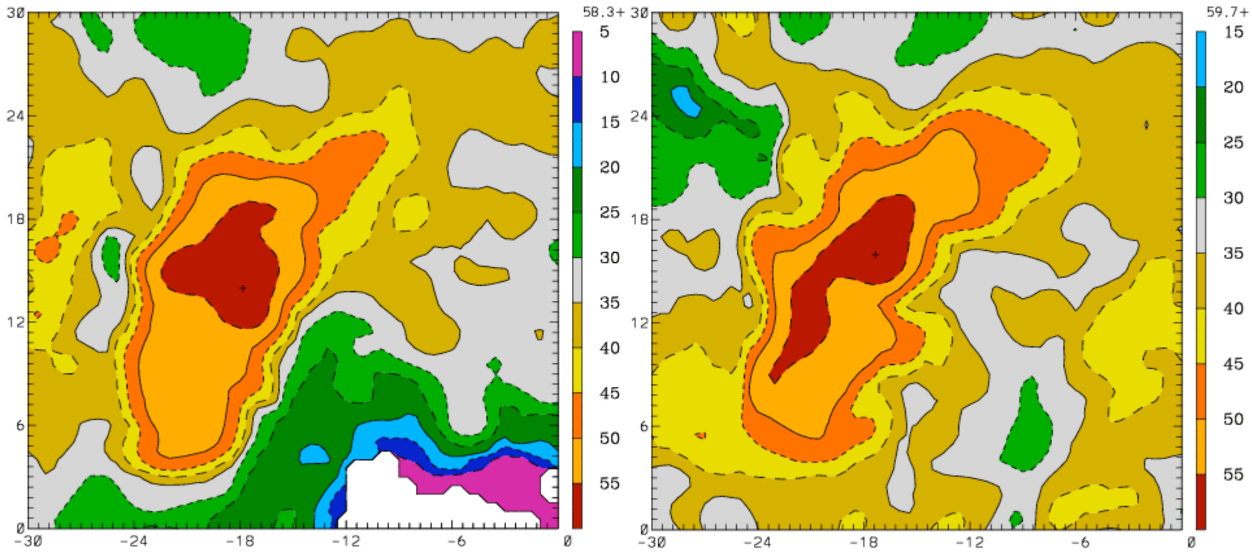

Fig. 9. *KOHX volume scan 1 (0655 UTC; left image) and volume scan 2 (0716 UTC; right image) taken at 3.0 km. Used for steadiness comparison between volume scans.*

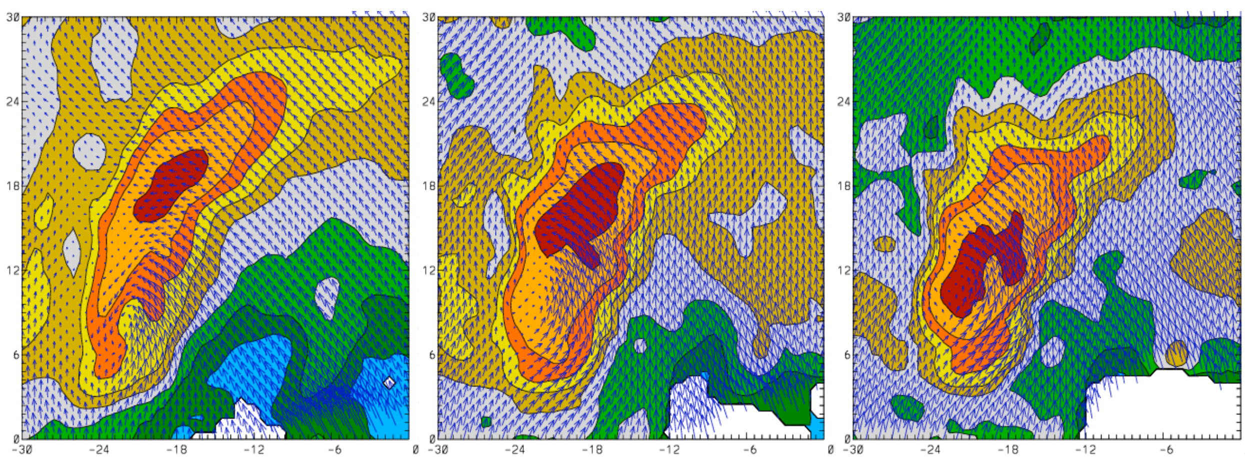

Fig. 10. *SDD analysis at 1.5, 3.0, and 4.0 km for case 2. Reflectivity scale is same as Fig. 9. Horizontal wind vectors are overlain. Reference vector -* 20 M/S

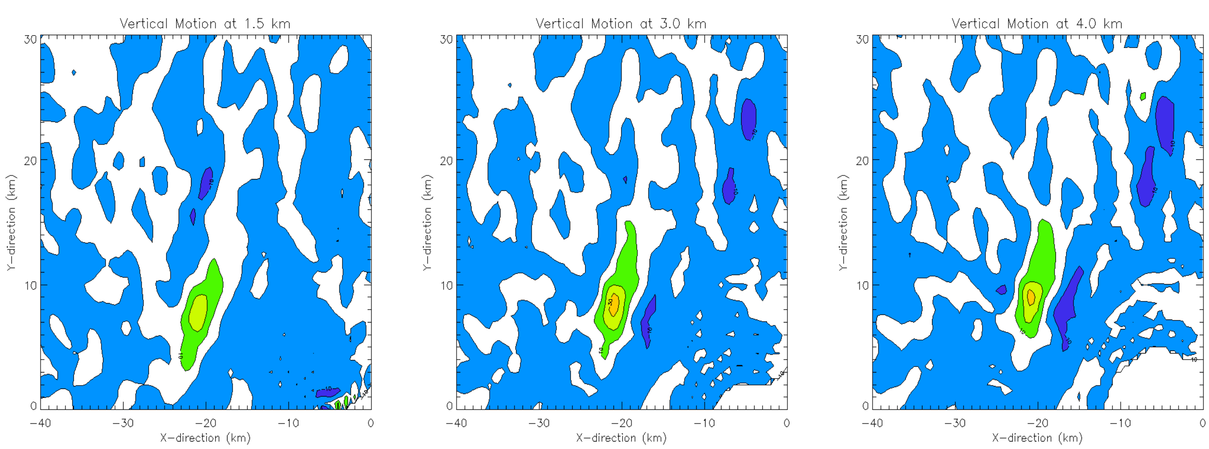

Fig. 11. *Vertical motion at 1.5, 3.0, and 4.0 km for case 2. Warm colors are positive (upward motion) and cool colors are negative (downward motion). Contour interval is 10 ms*$^{-1}$ *and green is ≥ +10 ms*$^{-1}$*. Note that Fig. 10 and 11 are not quite on the same scale.*

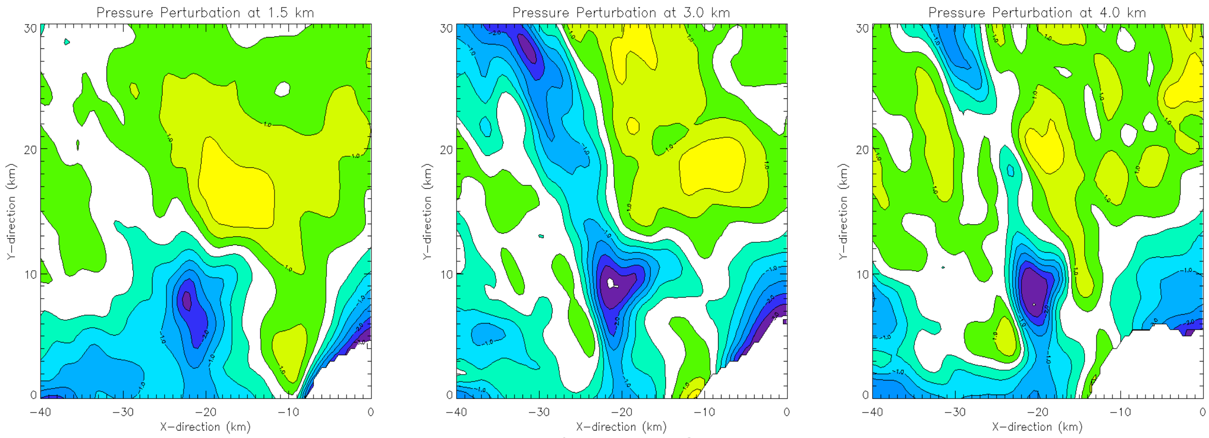

Fig. 12. *Pressure perturbation at 1.5, 3.0, and 4.0 km for case 2. Cool colors represent a negative perturbation while warm colors are positive. The contour interval is 0.5 hPa.*

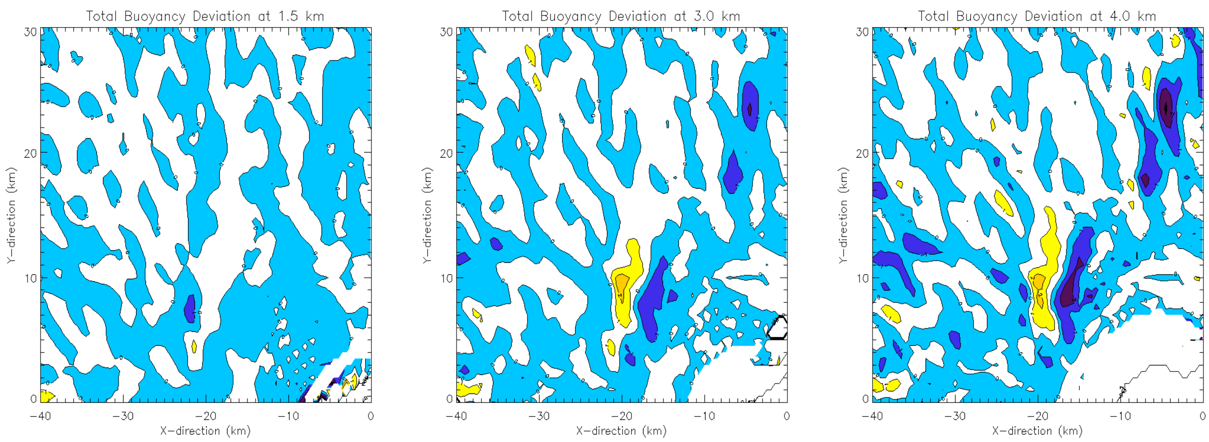

Fig. 13. *Total buoyancy deviations at 1.5, 3.0, and 4.0 km for case 2. Cool colors represent a negative deviation while warm a positive deviation. The contour interval is 1°.*

case 1. The vertical velocity pattern near the rear-flank gust front and RFD is not as well defined as case 1, however, there are still vertical velocities ≥ 10 ms^{-1} along the convergent boundary of the gust front at 1.5 and 3.0 km.

Pressure perturbations within the mesocyclone (Fig. 12) are similar to case 1 (-3.0 hPa), however, the local minima is located at 3.0 km - the location of the updraft maximum. Again, the location of the meso-low pressure indicates pressure gradient forcing helping maintain the updraft. Positive perturbations within the rear-flank are on the order of 0.5 to 1.5 hPa, and they begin appearing near 3.0 km.

Buoyancy deviations (Fig. 13) max out between +2.0 and +3.0 K (°C) at 3.0 km. The buoyancy fields are not as noisy as case 1, however, there are still issues near the radar baseline and data void regions. In contrast to case 1, the deviations are several degrees less.

For both cases, the relative locations and magnitudes of the mesocyclone, updraft maxima, pressure perturbation, and buoyancy deviation corresponded well with expectations. The cyclostropic balanced flow within the mesocyclone produced a low perturbation pressure near the center of the cyclonic circulation, as expected. Brandes (1984) found pressure perturbations up to -2 and -3 hPa just to the right of the mesocyclone, similar to what is found here. The buoyancy deviations (positive-negative couplet near the mesocyclone) also appear similar to those found by Brandes (1984), however the magnitude of case 1 is much greater. According to linear theory, a negative horizontal pressure gradient forms across the updraft in the direction of the environmental wind shear vector (Rotunno and Klemp 1982; Hane and Ray 1985; Cai and Wakimoto 2001), which appears to be the case here.

5. CONCLUSIONS

Given the visual comparison of volume scans, correlation analysis, and results from the analyses, the SDD analysis for case 2 (and thermodynamic retrievals) seems more accurate than case 1. The SDD analysis appears to capture the mesocyclone fairly well for the first case, however, due to the evolving nature of the storm, it's apparent that errors are unavoidable. If a subjective quality score had to be given, based on the results seen here, case 1 would rank a 2 and case 2 a 4, out of a possible 5.

Case 2, however, demonstrates just how reliable and accurate SDD analyses can be, given the requirements and assumptions are met. The feature needs to meet the steady-state assumption, as well as propagate at a close enough (but not too close) distance to a radar site, and at a quick enough speed to move through at least 30° of radar azimuth. It's often difficult to meet just one of these requirements with supercell thunderstorms, much less all of them. Often, supercells are evolving much to fast for a SDD analysis to be performed, which is why case 2 is unique.

If the results of case 1 can be considered reliable enough for a comparison, then there are several areas where these storms compare and contrast. Obviously, the mesocyclone of case 1 was stronger (seen by the stronger cyclonic circulation) than case 2, along with the updraft strength and level of updraft maximum (+50 ms^{-1} at 4 km vs. +34.5 ms^{-1} at 3 km). The buoyancy deviations were greater in case 1 (more than 4°), possibly leading to greater buoyancy forcing of the updraft. Features within the rear-flank (pressure perturbations, vertical velocities, etc.) were more distinguishable in case 1, which again points to a stronger supercell. Both storms had comparable pressure perturbations within the mesocyclone (near -3 hPa), however, the structure was quite different. Case 1 tended to have greater positive pressure perturbations, but most of this occurred in areas where data could be questionable. Overall, it is quite apparent that even though these supercells developed during the same event, environmental and internal differences played a significant role in their development.

Future work with this event include examining other storms from a single Doppler viewpoint to put these two in perspective. More SDD analyses will be performed, where possible. VAD analyses will also be used to reveal changes in SRH during storm passage (especially for the KOHX case) and details of storm outflow. A more robust thermodynamic retrieval would like to be performed, included retrieving variables such as temperature and theta deviations within the storms. Eventually, a high resolution numerical simulation will be used for further comparisons of the SDD analyses and thermodynamic retrievals.

6. ACKNOWLEDGEMENTS

This research was supported by NOAA grant NA08OAR4600896.

7. REFERENCES

Bluestein, H., and D. Hazen, 1989: Doppler-radar analysis of a tropical cyclone over land: Hurricane Alicia (1983) in Oklahoma. *Mon. Wea. Rev.*, **117**, 2594-2611.

Brandes, E. A., 1984: Relationships between radar-derived thermodynamic variables and tornadogenesis. *Mon. Wea. Rev.*, **112**, 1033-1052.

Cai, H. and R. M. Wakimoto, 2001: Retrieved pressure field and its influence on the propagation of a supercell thunderstorm. *Mon. Wea. Rev.*, **129**, 2695-2713.

Cressman, G. P., 1959: An operational objective analysis system. *Mon. Wea. Rev.*, **87**, 367-374.

Gal-Chen, T., 1978: A method for the initialization of the anelastic equations: Implications for matching models with observations. *Mon. Wea. Rev.*, **106**, 587-606.

Hane, C. E., and P. S. Ray, 1985: Pressure and buoyancy fields derived from Doppler radar data in a tornadic thunderstorm. *J. Atmos. Sci.*, **42**, 18-35.

_____, R. B. Wilhelmson and T. Gal-Chen, 1981: Retrieval of thermodynamic variables within deep convective clouds: Experiments in three dimensions. *Mon. Wea. Rev.*, **109**, 564-576.

Klimowski, B. A., and J. D. Marwitz, 1992: The synthetic dual-Doppler analysis technique. *J. Atmos. Oceanic Technol.*, **9**, 728-745.

Lhermitte, R. M., and L. J. Miller, 1970: Doppler radar methodology for the observation of convective storms. Preprints, *14th Conf. on Radar Meteorology*. Tucson, Amer. Meteor. Soc., 133-138.

Mohr, C. G., L. J. Miller, R. L. Vaughan, and H. W. Frank, 1986: Merger of mesoscale data sets into a common Cartesian format for efficient and systematic analysis. *J. Atmos. Oceanic Technol.*, **3**, 143-161.

Pasken, R., and Y. J. Lin, 1982: Pressure perturbations within a tornadic storm derived from dual-Doppler wind data. Preprints, *12th Conf. on Severe Local Storms*, San Antonio, Amer. Meteor. Soc., 257-260.

Rotunno, R., and J. B. Klemp, 1982: The influence of shear induced pressure gradient on thunderstorm motion. *Mon. Wea. Rev.*, **110**, 136-151.

Roux, F., 1985: Retrieval of thermodynamic fields from multiple-Doppler radar data using the equations of motion and thermodynamic equation. *Mon. Wea. Rev.*, **113**, 2142-2157.